Research Square

Preprints are preliminary reports that have not undergone peer review.
They should not be considered conclusive, used to inform clinical practice,
or referenced by the media as validated information.

Glyphosate Adsorption on H 3 PO 4 -Activated Biochars Derived from Maize Cob, Maize Husk and Coconut Fiber: Experimental, Thermodynamic and Computational Insights

James O. Nwagba

james.nwagba@abiastateuniversity.edu.ng

Abia State University

Jude C. Igwe

Abia State University

Anthony I. Obike

Abia State University

Kelechi E. Onwuka

Federal University of Technology Owerri

Franklin I. Udorji

Abia State University

Christopher U. Ahalibe

Abia State University

Research Article

Keywords: glyphosate, H3PO4-activated biochar, adsorption thermodynamics, density functional theory, agricultural residues

Posted Date: November 19th, 2026

DOI: https://doi.org/10.21203/rs.3.rs-11475586/v1

License: This work is licensed under a Creative Commons Attribution 4.0 International License.
Read Full License

Additional Declarations: No competing interests reported.

Glyphosate Adsorption on H_3PO_4-Activated Biochars Derived from Maize Cob, Maize Husk and Coconut Fiber: Experimental, Thermodynamic and Computational Insights

James O. Nwagba [1,*], Jude C. Igwe[1*], Anthony I. Obike[1], Kelechi E. Onwuka [2], Franklin I. Udorji[1] Christopher U. Ahalibe

[1]*Department of Pure and Industrial Chemistry, Abia State University, Uturu, Nigeria*

[2]*Department of Pure and Applied Chemistry, Federal University of Technology, Owerri, Nigeria*

*Corresponding authors: james.nwagba@abiastateuniversity.edu.ng; jude.igwe@abiastateuniversity.edu.ng

Abstract

Glyphosate is a widely used herbicide whose residues contaminate water, and researchers are investigating biochars derived from agricultural residues for its removal. In this study, we characterized H3PO4-activated biochars from maize cob (MCA), maize husk (MHA), and coconut fiber (CFA), as well as their unactivated counterparts, by surface area, pore volume, density, conductivity, cation exchange capacity, FTIR, and SEM. Activation increased the surface area from 12.5–25.8 to 75.4–102.7 $m^2\ g^{-1}$ and the pore volume from 0.028–0.085 to 0.635–1.125 $cm^3\ g^{-1}$. Glyphosate adsorption (2.0 g L^{-1}; natural pH 4.67) was monitored by direct UV–Vis at 210 nm. After 120 min at 10 mg L^{-1}, the activated biochars removed 78.0–87.7% of glyphosate (q_e = 3.90–4.39 mg g^{-1}), compared with 35.0–51.6% for the unactivated chars. At 100–500 mg L^{-1}, the apparent uptake of the activated biochars reached at least 212 mg g^{-1} at 500 mg L^{-1} without a plateau; since this exceeds published capacities and part of the data fall below the calibrated range, these values are considered provisional. For the activated biochars, removal at 10 mg L^{-1} increased with temperature between 15 and 45 °C, and Van't Hoff analysis yielded negative $\Delta G°$ (−7.6 to −15.1 kJ mol^{-1}), positive $\Delta H°$ (+34.8 to +54.5 kJ mol^{-1}), and positive $\Delta S°$ (+153 to +219 J $mol^{-1}\ K^{-1}$). Gas-phase DFT of neutral glyphosate (B3LYP/6-31G) identified the oxygen atoms as the most negative sites, and GFN2-xTB screening on functional-group models produced adsorption energies of −19 to −52 kJ mol^{-1} for the glyphosate monoanion expected at pH 4.67, within the physisorption range. These results support a spontaneous, endothermic uptake involving hydrogen bonding and electrostatic interaction with surface oxygen and phosphorus groups, although the mechanism is not conclusively demonstrated. The quantitative findings should be validated with an independent analytical method and appropriate controls.

Keywords: glyphosate; H_3PO_4-activated biochar; adsorption thermodynamics; density functional theory; agricultural residues

1. Introduction

Glyphosate (N-(phosphonomethyl)glycine) is among the most widely used herbicides worldwide, applied at rates of hundreds of thousands of tons per year (Bai & Ogbourne, 2016). In Nigeria, it is one of the most commonly used herbicides (Oyetunji et al., 2024), and residues of glyphosate and its metabolites have been found in market-sold African catfish in Ibadan at levels above the acceptable daily intake and maximum residue limit used by the authors (Alarape et al., 2023). Glyphosate and its degradation product AMPA occur frequently and widely in surface water, groundwater, and precipitation (Battaglin et al., 2014). In 2015, the International Agency for Research on Cancer classified glyphosate as probably carcinogenic to humans (Group 2A) (Guyton et al., 2015). Its small size, polarity, and high water solubility make it mobile once released (Borggaard & Gimsing, 2008), so low-cost treatment options for contaminated water are needed.

Adsorption is attractive because it is simple and scalable and, unlike some oxidative or membrane routes, does not generate secondary pollutants (Cosgrove et al., 2019; Ighalo et al., 2021). Biochars have been tested for glyphosate removal with varied results. A steam-activated rice husk biochar reached a Langmuir capacity of 123.03 mg g^{-1}, and Herath et al. (2016) proposed pore diffusion, π–π electron donor–acceptor interactions, hydrogen bonding, and electrophilic interactions as the controlling mechanisms. Mayakaduwa et al. (2016) examined a woody biochar using equilibrium and kinetic mechanisms, and Sen et al. (2019) characterized an orthophosphoric acid-modified eucalyptus bark char using pHpzc, surface analysis, and FTIR, along with isotherm, thermodynamic, and Box–Behnken optimization results. Biochars from açaí-seed residue and from Fe_3O_4-loaded coffee husk have also been evaluated (Zaparoli et al., 2023; Lita et al., 2023), and an H_3PO_4-oxidised corn cob biochar removed about 53% of a commercial glyphosate formulation, with a capacity of 1.49 mg g^{-1} (Marcelino et al., 2022).

Chemical activation with phosphoric acid before carbonization develops porosity and introduces phosphorus- and oxygen-containing surface groups, which can increase surface area and provide specific binding sites (Jagtoyen & Derbyshire, 1993; Ioannidou & Zabaniotou, 2007; Yakout & Sharaf El-Deen, 2016). Maize cob, maize husk, and coconut fiber are lignocellulosic residues from crops grown in Nigeria, and comparative data on their H3PO4-activated biochars for glyphosate removal appear limited.

Glyphosate adsorption is also strongly shaped by its speciation. The molecule carries phosphonic, carboxylic, and amine groups, with reported pK_a values spanning roughly 0.8 to 11 (Borggaard & Gimsing, 2008; Liu et al., 2016; ATSDR, 2021), so its charge changes with solution pH (Figure 2). Mechanisms for biochars have mostly been inferred from fitted isotherm and kinetic models and from FTIR shifts. Such inferences describe how uptake behaves but cannot identify the binding sites. Thermodynamic parameters (ΔG°, ΔH°, ΔS°) and activation energies provide insight into spontaneity

and energetics, provided the equilibrium constant is made dimensionless before use in the van't Hoff equation (Lima et al., 2019).

Density functional theory (DFT) can test these inferences at the molecular level. Araújo et al. (2024) combined ab initio molecular dynamics and DFT with FTIR and Raman spectroscopy for glyphosate on graphene-based materials and found physisorption on pristine and doped regions, but chemisorption with molecular dissociation at vacancy-type defects. Published adsorption energies of glyphosate on carbon-based surfaces range from about −0.3 eV on nitrogen-doped or pristine graphene to about −1.6 eV on metal-decorated graphene (Hernández-Barreto et al., 2022), and doping with Fe^{3+} or Al^{3+} strengthens binding through cooperative non-covalent and coordinative interactions (Mojica-Sánchez et al., 2026). In the present work, DFT is used for glyphosate itself to identify its likely interaction sites, and semi-empirical GFN2-xTB calculations on functional-group models of the activated surface are used to estimate adsorption energies, which are compared with the experimental thermodynamics and with these published energies; DFT refinement of the adsorption energies is left to follow-up work.

This study therefore examines glyphosate adsorption onto H_3PO_4-activated biochars prepared from maize cob (MCA), maize husk (MHA) and coconut fiber (CFA). Specifically, we

(i) Characterize the three biochars by surface area, pore volume, density, conductivity, cation exchange capacity, FTIR and SEM;

(ii) Quantify uptake as a function of contact time and initial concentration at the natural pH (4.67) of the glyphosate solution and a fixed adsorbent dose of 2.0 g L^{-1};

(iii) Analyze kinetics, equilibrium, and thermodynamics from experiments at 15, 30, and 45 °C; and

(iv) Use gas-phase DFT to compute the geometry, reactivity descriptors, and charge distribution of glyphosate, and GFN2-xTB calculations on functional-group models to estimate adsorption energies for comparison with the experimental thermodynamics.

This paper does not cover the effects of solution pH, fixed-bed column performance, or adsorbent regeneration; other pesticides studied in the wider project are reported separately.

2. Materials and Methods

2.1 Chemicals and reagents

Analytical-grade glyphosate (≥ 98 %) was used throughout. Phosphoric acid (85 % w/w), hydrochloric acid, and other reagents, all supplied by Afrimash Company Limited (Aba, Abia State), were used as received. All solutions were prepared in ultra-pure water. We did not use commercial formulations because their surfactants and co-formulants can interfere with both adsorption and analysis.

2.2 Preparation of H_3PO_4-activated biochars

We collected maize cob, maize husk, and coconut fiber from farms and markets in Uturu, Isuikwuato LGA, Abia State, Nigeria. They were washed, shade-dried for 14 days, ground in a mechanical grinder, and sieved to < 2 mm. Each powder was impregnated with 85 wt. % H_3PO_4 at a 1:1 (w/v) ratio (such that 100 g of dried biomass sample was mixed with 100 mL of the acid solution) for 24 h at room temperature. The mixture was then carbonized in a muffle furnace at 500 °C for 1 h under N_2 gas flowing at a rate of 150 mL min^{-1} with a controlled furnace heating rate of 10 °C min^{-1}. After cooling under N_2 flow, the products were washed sequentially with hot deionized water and 0.1 M HCl until the filtrate conductivity stabilized and the wash water reached pH 7.0. The washed biochars were dried at 110 °C for 12 h and stored in airtight containers. We prepared unactivated reference chars (designated MC, MH, and CF) by carbonizing the raw biomass precursors under identical thermal conditions (500 °C for 1 h under N_2 flow) but without the chemical impregnation step. The final activated biochars are designated MCA (maize cob activated), MHA (maize husk activated) and CFA (coconut fiber activated). The workflow is shown in Figure 1.

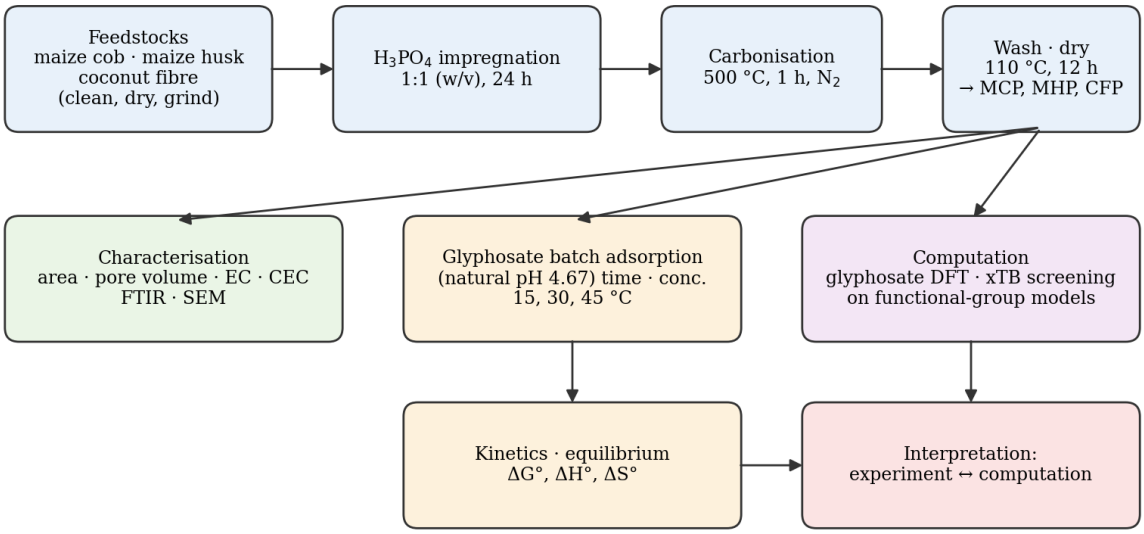


Figure 1. Overall study workflow, from feedstock preparation to the integrated experimental–DFT mechanism.

2.3 Characterization

An external analytical laboratory measured the physical and chemical properties of the unactivated (MC, MH, CF) and activated (MCA, MHA, CFA) chars. Specific surface area was estimated by the Sears titration method (Sears, 1956): 0.1 g of adsorbent was suspended in 25 mL of 1 M NaCl, the pH was adjusted to 3–4 with 0.1 M HCl, and the suspension was titrated with 0.1 M NaOH to pH 9; the surface area (S, $m^2\ g^{-1}$) was calculated as $S = 32.0V - 25$, where V is the volume of NaOH (mL) needed to raise the pH from 4 to 9. Pore volume was determined by the liquid volume of N_2 adsorbed at a single

maximum relative pressure (P/P_0) of 0.99. We measured particle density with a water pycnometer and bulk density as the mass of sample per unit volume after tapping in a 50 mL graduated cylinder until the level no longer fell. Electrical conductivity was measured on the clear supernatant of 0.1 g of sample agitated in 20 mL of deionized water for 1 h. Cation exchange capacity was estimated from exchangeable Ca, Mg, and K measured by atomic absorption spectrophotometry as Ca/200 + Mg/120 + K/390. The Sears surface area is an indirect, titration-based estimate used here to compare the samples; it is not equivalent to a BET area from N2 adsorption, which we did not measure.

We recorded surface functional groups of the glyphosate-loaded biochars on a PerkinElmer FTIR spectrometer with a DTGS detector over 4000–400 cm^{-1} using attenuated total reflection (ATR) sampling, accumulating 32 scans at a resolution of 4 cm^{-1}. We examined morphology by scanning electron microscopy using a JEOL JSM-6510LV SEM at an accelerating voltage of 20 kV in low-vacuum mode (70 Pa), without prior conductive coating.2.4 Glyphosate solutions and quantification

A glyphosate stock solution of 1000 mg L^{-1} was prepared in ultra-pure water and diluted to the working concentrations. We measured glyphosate by direct UV–Vis spectrophotometry on a Shimadzu UV-1900i at 210 nm in quartz cuvettes against ultra-pure water. Glyphosate has no strong chromophore, so direct UV quantification is not specific: absorbance near 210 nm can also arise from other species, such as organic matter or phosphate leached from the biochars, and glyphosate is therefore often determined after derivatization (Bhaskara & Nagaraja, 2006). Two calibration curves were used (Figure 3): 2–10 mg L^{-1} for the time and temperature studies ($A = 0.09261C + 0.0004$, $R^2 = 1.00000$), and 50–500 mg L^{-1} for the concentration study ($A = 0.2083 + 0.002592C$, $R^2 = 0.9976$). Concentrations were calculated from these regression equations, including the intercept, and samples were read undiluted. The standard absorbances were taken from the plotted calibration curves in the laboratory report. In the concentration study, samples with an absorbance below that of the 50 mg L^{-1} standard (0.338) fall below the calibrated range, and for these only an upper limit of 50 mg L^{-1} could be assigned to the equilibrium concentration. Key properties of glyphosate and the analytical settings are in Table 1.

Table 1. Properties of glyphosate and analytical settings.

Property	**Value**
Formula; molar mass	$C_3H_8NO_5P$; 169.07 g mol^{-1} (PubChem, CID 3496)
Water solubility	≈ 1.01 g per 100 mL at 20 °C (Sen et al., 2019); about 12 g L^{-1} at 25 °C is also reported
Acid dissociation	pK_a < 2 (phosphonic), 2.6 (carboxylic), 5.6 (phosphonic), and 10.6 (amine) (ATSDR, 2021); other compilations give 0.8, 2.3, 6.0, and 11.0
Log K_{ow}	−3.2 to −3.4, strongly hydrophilic (Tzilivakis et al., 2026; PubChem)
Detection	Direct UV–Vis (Shimadzu UV-1900i), λ = 210 nm; quartz cuvettes

Property	Value
Calibration and QC	Two curves: 2–10 mg L^{-1} (R^2 = 1.00000) and 50–500 mg L^{-1} (R^2 = 0.9976); LOD = 10.50 and LOQ = 31.80 mg L^{-1} as 3.3σ/S and 10σ/S; spike recovery range of 94.2% to 103.5% across all tested biochar %

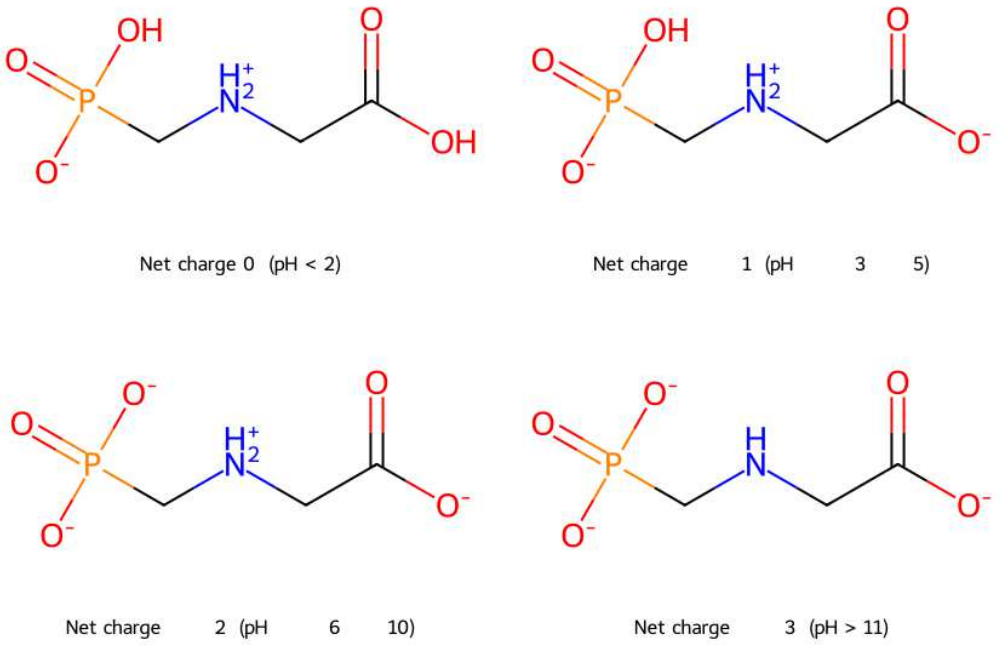


Figure 2. Dominant ionization states of glyphosate with increasing pH, using the pK_a values of < 2, 2.6, 5.6, and 10.6 (ATSDR, 2021). Gas-phase DFT calculations do not define a pH, so the neutral species is used as the reference form in Section 2.8.

The standard curve of glyphosate is shown in Figure 3. We filtered samples through 0.45 µm membranes and assessed possible adsorptive loss on the filter.

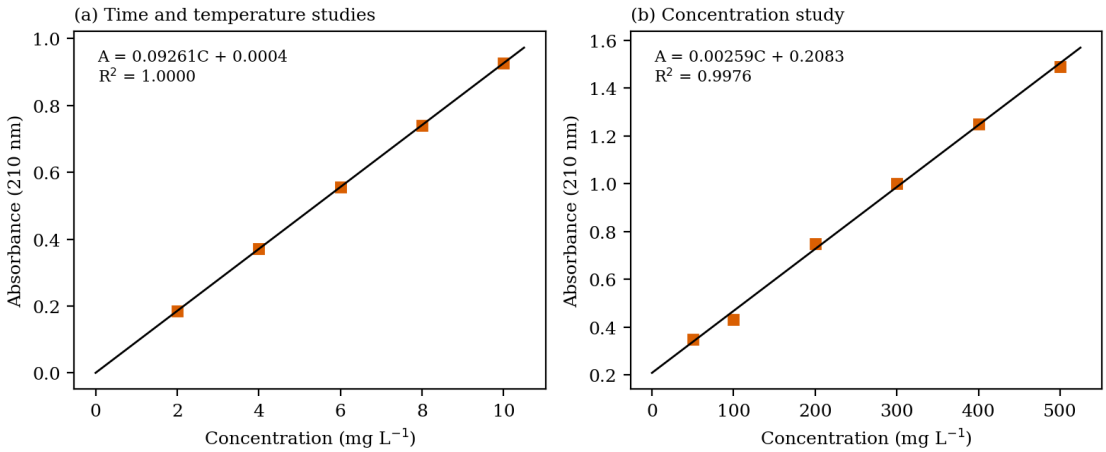


Figure 3. Calibration curves for glyphosate at 210 nm: (a) 2–10 mg L^{-1} standards used for the time and temperature studies; (b) 50–500 mg L^{-1} standards used for the concentration study. Lines are linear regressions with intercept.

2.5 Batch adsorption experiments

Batch experiments used 100 mL capped flasks containing 0.20 g of adsorbent in 100 mL of glyphosate solution (dose 2.0 g L^{-1}), agitated at 200 rpm in a temperature-controlled orbital shaker. The solutions were used at their natural pH of 4.67, which was not varied or adjusted, so the effect of pH was not investigated (Section 3.7). Three studies were run. In the contact-time study, 10 mg L^{-1} glyphosate was sampled at 10, 30, 50, 90, and 120 min at 25 ± 2 °C. In the concentration study, we sampled initial concentrations of 100, 200, 300, 400, and 500 mg L−1, prepared by diluting the 1000 mg L−1 stock, after 120 min at 25 ± 2 °C. In the temperature study, 10 mg L^{-1} glyphosate was held at 15, 30 and 45 °C (288.15, 303.15 and 318.15 K) within ±0.5 °C for 120 min. Aliquots were filtered and read at 210 nm as in Section 2.4.

Glyphosate-only (no adsorbent) and adsorbent-only controls were not included in this series, so loss of glyphosate to glassware and absorbance from species leached by the chars were not corrected. Each absorbance in the laboratory report is the mean of three readings; standard deviations are not reported. The amount adsorbed at time t and at equilibrium, and the removal efficiency, were calculated as:

$$q_t = \frac{(C_0 - C_t)V}{m} \quad (1)$$

$$q_e = \frac{(C_0 - C_e)V}{m} \quad (2)$$

$$R(\%) = \frac{(C_0 - C_e)}{C_0} \times 100 \quad (3)$$

Where C_0, C_t, and Ce (mg L−1) are the initial, time-t, and equilibrium concentrations; V (L) is the solution volume; and m (g) is the adsorbent mass.

Table 2. Experimental design for the batch adsorption study.

Factor	Levels/conditions
Adsorbents	MCA, MHA, CFA
Adsorbate	Glyphosate (single-solute solutions; 1000 mg L^{-1} stock)
Adsorbent dose	0.20 g per 100 mL (2.0 g L^{-1}), fixed
Initial concentration	10 mg L^{-1} (time and temperature studies); 100, 200, 300, 400 and 500 mg L^{-1} (concentration study)
Contact time	10, 30, 50, 90 and 120 min (time study); 120 min (concentration and temperature studies)
Temperature	15, 30 and 45 °C (temperature study; 288.15, 303.15, 318.15 K); 25 ± 2 °C (room temperature) for the time and concentration studies
Solution pH	Natural pH 4.67 (not varied or adjusted)
Agitation	200 rpm
Replication and controls	Each absorbance is the mean of three readings (laboratory report); controls not included.

2.6 Kinetic and isotherm modeling

Kinetic data were fitted with the pseudo-first-order (Lagergren, 1898), pseudo-second-order (Ho & McKay, 1999), Elovich and intraparticle diffusion models and, where the data allowed, equilibrium data with the Langmuir, Freundlich, Temkin and Dubinin–Radushkevich (D–R) models (Table 3; the limits of the equilibrium data are described in Section 3.3). All model optimizations were performed by non-linear regression with custom scripts in Python 3 using the Trust Region Reflective algorithm in scipy.optimize.curve_fit v1.12.0, following recommended practice for fitting and reporting in adsorption studies (Tran et al., 2017). Goodness of fit was evaluated from the adjusted coefficient of determination (adj-R^2), the root mean square error (RMSE), and the chi-square statistic (χ^2):

$$RMSE = \sqrt{\frac{\sum_{i=1}^{n}\left(q_{exp}-q_{cal}\right)^2}{n-p}} \tag{4}$$

$$\chi^2 = \sum_{i=1}^{n}\frac{\left(q_{exp}-q_{cal}\right)^2}{q_{cal}} \tag{5}$$

Where q_{exp} and q_{cal} are the experimental and model-calculated uptakes, n is the number of data points, and p is the number of model parameters. The best model had the lowest RMSE and χ^2, the highest adjusted R2, and also gave physically meaningful parameters.

Table 3. Kinetic and isotherm models used.

Model	**Nonlinear equation**	**Parameters**
Pseudo-first-order	$qt = qe(1 - e - k^1 t)$	$k^1(min - 1)$
Pseudo-second-order	$qt = \frac{k^2 qe2t}{(1 + k^2 qet)}$	$k^2(g\ mg - 1\ min - 1)$
Elovich	$qt = \left(\frac{1}{\beta}\right)\ln(1 + \alpha\beta t)$	α initial rate; β related to surface coverage
Intraparticle diffusion	$qt = \frac{kidt1}{2} + C$	k_{id}; C (boundary-layer effect)
Langmuir	$qe = \frac{qmKLCe}{(1 + KLCe)}$; $RL = \frac{1}{1 + KLC0}$	$qm\ (mg\ g - 1)$; $KL\ (L\ mg - 1)$; RL (favorability)
Freundlich	$qe = \frac{KFCe1}{n}$	$KF; \frac{1}{-n}$ (heterogeneity)
Temkin	$qe = \left(\frac{RT}{bT}\right)\ln(ATCe)$	b_T (heat of adsorption); A_T
Dubinin–Radushkevich	$qe = qmexp(-\beta\varepsilon 2)$; $\varepsilon = RT\ln\left(1 + \frac{1}{Ce}\right)$; $E = \frac{1}{\sqrt{(2\beta)}}$	$E\ (kJ\ mol - 1)$, mean free energy

2.7 Thermodynamics

Thermodynamic parameters were obtained from the temperature study at 15, 30 and 45 °C (288.15, 303.15 and 318.15 K) using:

$$\Delta G° = -RT\ ln\ K_c \tag{6}$$

$$ln\ K_c = \frac{\Delta S°}{R} - \frac{\Delta H°}{RT} \tag{7}$$

$$\Delta G° = \Delta H° - T\Delta S° \tag{8}$$

Where K_c is the dimensionless equilibrium constant, R = 8.314 J mol^{-1} $K^{-1,}$ and T is the absolute temperature. At each temperature, the equilibrium distribution coefficient $K_d = q_e/C_e$ (L g^{-1}) was converted to a dimensionless constant following Lima et al. (2019):

$$K_c = \frac{K_d \times M_{Gly} \times [Gly]°}{\gamma} \tag{9}$$

Where M_{Gly} = 169.07 g mol^{-1}, Gly° = 1 mol L^{-1} is the standard-state concentration, and γ is the activity coefficient of the adsorbate (taken as 1 for dilute solution). Isotherms were not measured at each temperature, so K_c was derived from the single initial concentration of 10 mg L^{-1}, which lies in the low-coverage region. ΔH° and ΔS° were obtained from the slope and intercept of ln K_c against 1/T, and with three temperatures the regression R^2 and the standard errors of ΔH° and ΔS° are reported. Activation energies could not be derived because rate constants were measured at one temperature only.

2.8 Computational (DFT) methods

2.8.1 Glyphosate geometries and reactivity descriptors

Structures were drawn in ChemSketch, converted to 3D models in Avogadro and optimized in Gaussian 09 Revision D.01 (Frisch et al.) at the B3LYP level (Becke, 1993; Lee et al., 1988) with the 6-31G basis set (110 basis functions), in the gas phase and without a dispersion correction. The optimized species is neutral glyphosate in its closed-shell singlet state (charge 0; 18 atoms). Because the calculation is in the gas phase, pH is not defined, and we use the neutral form as the reference species; therefore, the pH-dependent speciation in water (Figure 2) is not represented. The optimization was not followed by a frequency calculation. From the HOMO and LUMO energies of the optimized structure, the following descriptors were calculated (Parr & Pearson, 1983; Parr et al., 1999), together with the energy gap (ΔE = $E_{LUMO} - E_{HOMO}$) and electronegativity (χ = −μ):

$$\mu = \frac{E_{HOMO}+E_{LUMO}}{2} \tag{10}$$

$$\eta = \frac{E_{LUMO}-E_{HOMO}}{2} \tag{11}$$

$$\omega = \frac{\mu^2}{2\eta} \tag{12}$$

$$\sigma = \frac{1}{\eta} \tag{13}$$

Molecular electrostatic potential (MEP) maps were generated in GaussView.

2.8.2 Adsorption energies (semi-empirical screening)

Adsorption of glyphosate was screened on four functional-group models of the activated surface: pristine coronene ($C_{24}H_{12}$; S0), and coronene flakes with two hydroxyl groups and one carboxyl group (S1), two aryl phosphate groups, –O–P(=O)$(OH)_2$ (S2), and one hydroxyl, one carboxyl, and one aryl phosphate group (S3). These groups represent the hydroxyl, carbonyl/carboxyl, and P–O–C/P=O functions suggested by the FTIR spectra and by H_3PO_4 activation; they are generic models and are not specific to a feedstock. Glyphosate was taken as the neutral molecule (in vacuum and in implicit water) and as the monoanion expected at the natural pH of 4.67 (in implicit water). Geometries were optimized with the GFN2-xTB method (tblite) and the ALPB implicit-water model, using the L-BFGS algorithm in ASE (maximum force 0.06 eV Å^{-1}, at most 400 steps). For each model and species, five random

starting orientations of glyphosate were generated (heights of 3–7 Å above either face of the flake, with 60% of the starts directed at the O and P atoms of the groups), and the lowest-energy complex is reported. The adsorption energy was calculated as:

$$E_{ads} = E_{complex} - E_{surface} - E_{glyphosate} \quad (14)$$

Each component is optimized in the same medium, and the most stable of the six conformers is taken as the isolated glyphosate molecule. The energies are GFN2-xTB electronic energies without counterpoise or thermal corrections. GFN2-xTB is a semi-empirical tight-binding method parametrized against DFT data, so these results are screening-level estimates; B3LYP-D3 (BJ)/6-31G counterpoise single-point calculations on the optimized geometries are planned.

Table 4. Summary of the computational protocols.

Item	**Setting**
Software	Gaussian 09 Revision D.01; GaussView and ASE (adsorption screening)
Method	B3LYP
Dispersion	None
Basis set	6-31G
Solvation	Gas phase (no solvent), 0 K electronic energies
Glyphosate species	Neutral, closed-shell singlet (charge 0)
Adsorption screening	GFN2-xTB (tblite); ALPB implicit water; ASE L-BFGS; four models; five starting orientations per case
Properties	Optimized geometry; HOMO/LUMO, ΔE, μ, η, ω, σ; Mulliken charges; dipole moment; MEP

3. Results and Discussion

3.1 Characterization of the biochars

Activation with H_3PO_4 changed the physical properties of all three feedstocks markedly (Table 5). Specific surface area (Sears titration) rose from 25.8, 18.3 and 12.5 $m^2\ g^{-1}$ for the unactivated chars MC, MH and CF to 95.5, 75.4 and 102.7 $m^2\ g^{-1}$ for MCA, MHA and CFA, which are increases of 3.7-, 4.1- and 8.2-fold. Pore volume increased more strongly, from 0.035, 0.028 and 0.085 $cm^3\ g^{-1}$ to 0.712, 0.635 and 1.125 $cm^3\ g^{-1}$. Among the activated biochars, both surface area and pore volume followed the order CFA > MCA > MHA. Particle density rose slightly with activation (1.41 to 1.52, 1.38 to 1.49 and 1.32 to 1.55 g cm^{-3}), whereas bulk density fell for maize cob and maize husk (0.52 to 0.35 and 0.48 to 0.32 g cm^{-3}) and changed little for coconut fiber (0.25 to 0.28 g cm^{-3}). The ratio of pore volume to

surface area gives a mean pore width (4V/S) of about 30–44 nm for the activated biochars (which would place the porosity in the mesopore–macropore range; this is an indicative estimate, because the surface area was obtained by titration).

Electrical conductivity of the supernatant increased on activation (185 to 350, 165 to 450 and 220 to 950 μS cm^{-1}), most strongly for CFA, which indicates a larger pool of soluble ionic species possibly residual phosphate and mineral salts retained after washing. Such leachates can contribute to the background of the UV assay, and, because no adsorbent-only blanks were run (Section 2.5), this contribution could not be corrected. Cation exchange capacity also rose on activation (22.4 to 48.2, 19.8 to 41.5 and 16.3 to 35.1 cmol kg^{-1}), which is consistent with more acidic oxygen- and phosphorus-containing surface groups created by H_3PO_4 activation.

Table 5. Properties of the unactivated (MC, MH, CF) and H_3PO_4-activated (MCA, MHA, CFA) chars. Laboratory IDs MCA, MHA and CFA correspond to MCA, MHA and CFA. Surface area by Sears titration; d_{avg} = 4V/S is calculated here.

Sample (lab ID)	Surface area (m^2 g^{-1})	Pore volume (cm^3 g^{-1})	d_{avg} (nm)	Particle density (g cm^{-3})	Bulk density (g cm^{-3})	Conductivity (μS cm^{-1})	CEC (cmol kg^{-1})
MC	25.8	0.035	5.4	1.41	0.52	185	22.4
MCA	95.5	0.712	29.8	1.52	0.35	350	48.2
MH	18.3	0.028	6.1	1.38	0.48	165	19.8
MHA	75.4	0.635	33.7	1.49	0.32	450	41.5
CF	12.5	0.085	27.2	1.32	0.25	220	16.3
CFA	102.7	1.125	43.8	1.55	0.28	950	35.1

The FTIR spectra of the glyphosate-loaded biochars (Figure 4) show broad O–H/N–H stretching bands between about 3376 and 3437 cm^{-1}, weak aliphatic C–H stretching bands near 2918–2927 cm^{-1}, C=O bands at 1709–1724 cm^{-1} for MHA, MC and CFA, strong bands between 1595 and 1643 cm^{-1} (tentatively aromatic C=C, carboxylate and N–H bending), bands near 1369–1384 cm^{-1} and 1285–1320 cm^{-1} (C–H bending, carboxylate and P=O) and bands between 1029 and 1103 cm^{-1} (P–O–C, P–O–P and C–O stretching). The features near 2352–2360 cm^{-1} come from atmospheric CO_2. Spectra before adsorption are not available, so bands of the biochars and of adsorbed glyphosate overlap, notably the carboxylate and phosphonate vibrations near 1600 and 1000–1100 cm^{-1}, and shifts on adsorption cannot be assessed.

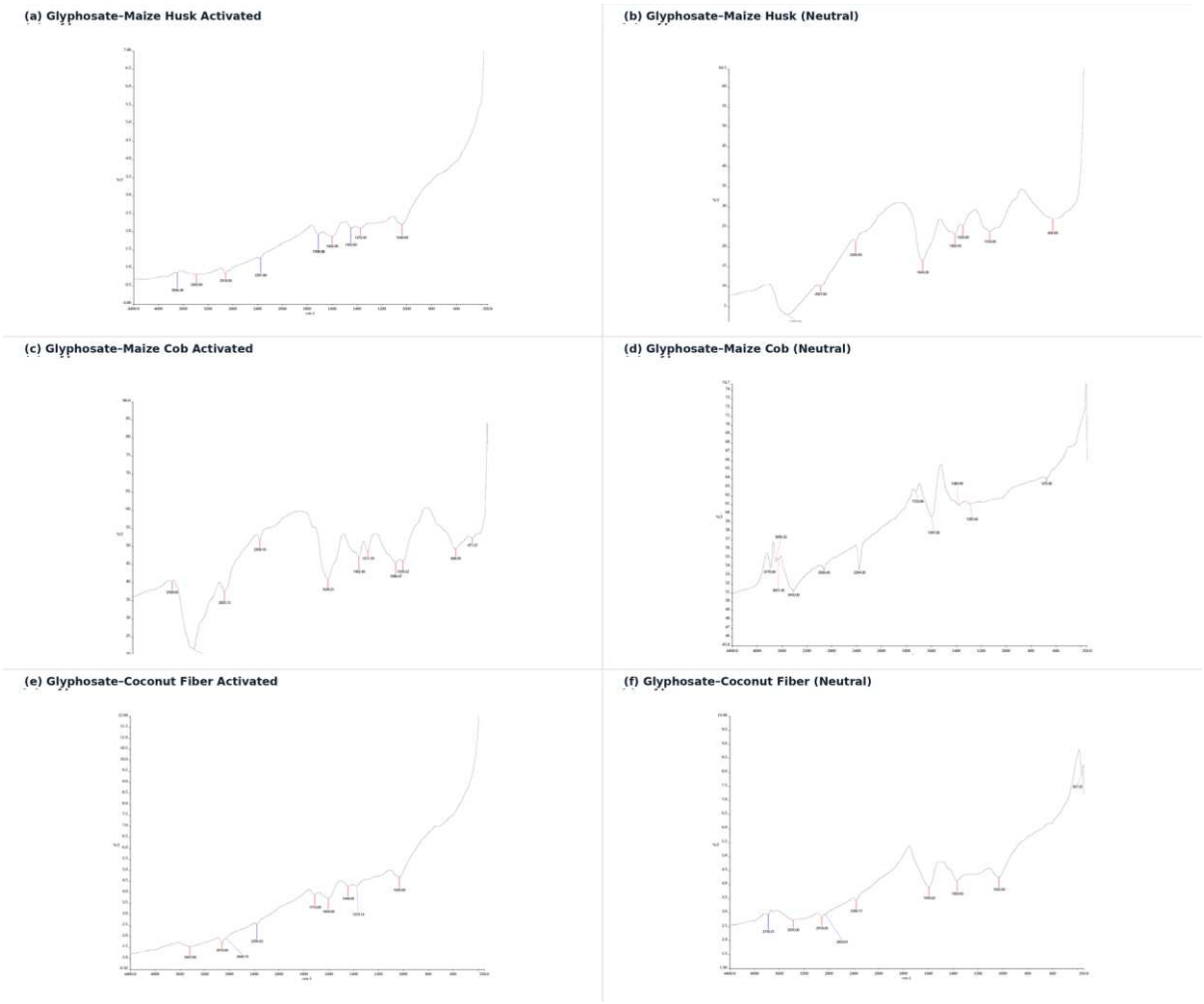


Figure 4. FTIR spectra of the glyphosate-loaded biochars: (a) activated maize husk (MHA), (b) maize husk (MH), (c) activated maize cob (MCA), (d) maize cob (MC), (e) activated coconut fibre (CFA) and (f) coconut fibre (CF). Peak positions (cm^{-1}) are those labelled by the instrument software. Panels (b), (d) and (f) show the unactivated chars (labelled "Neutral" in the panel titles).

SEM micrographs of the six samples (Figure 5) show that H_3PO_4 activation changed the surface morphology of each feedstock. The unactivated maize cob (MC) consisted of rough, layered and fibrous fragments with a compact, plate-like texture, whereas the activated maize cob (MCP) was made of rounded, aggregated grains with open voids between them. The unactivated maize husk (MH) appeared as fine, loosely packed particles, while the activated maize husk (MHP) showed a rougher, more fibrous, lamellar surface with many crevices and openings. The unactivated coconut fiber (CF) retained a thin-walled, cellular structure with large open cavities, which was replaced in the activated coconut fiber (CFP) by smooth, rounded, partly fused particles forming an aggregated network with voids between them. These observations are consistent with the more developed porosity and larger surface area of the activated biochars (Table 5), although SEM at these magnifications shows only the macroscopic texture and does not resolve micropores or quantify porosity. The micrographs were recorded at different

magnifications (5,000–7,000×) and fields of view, as indicated on each image, and SEM images after glyphosate adsorption were not obtained, so changes in adsorption cannot be assessed.

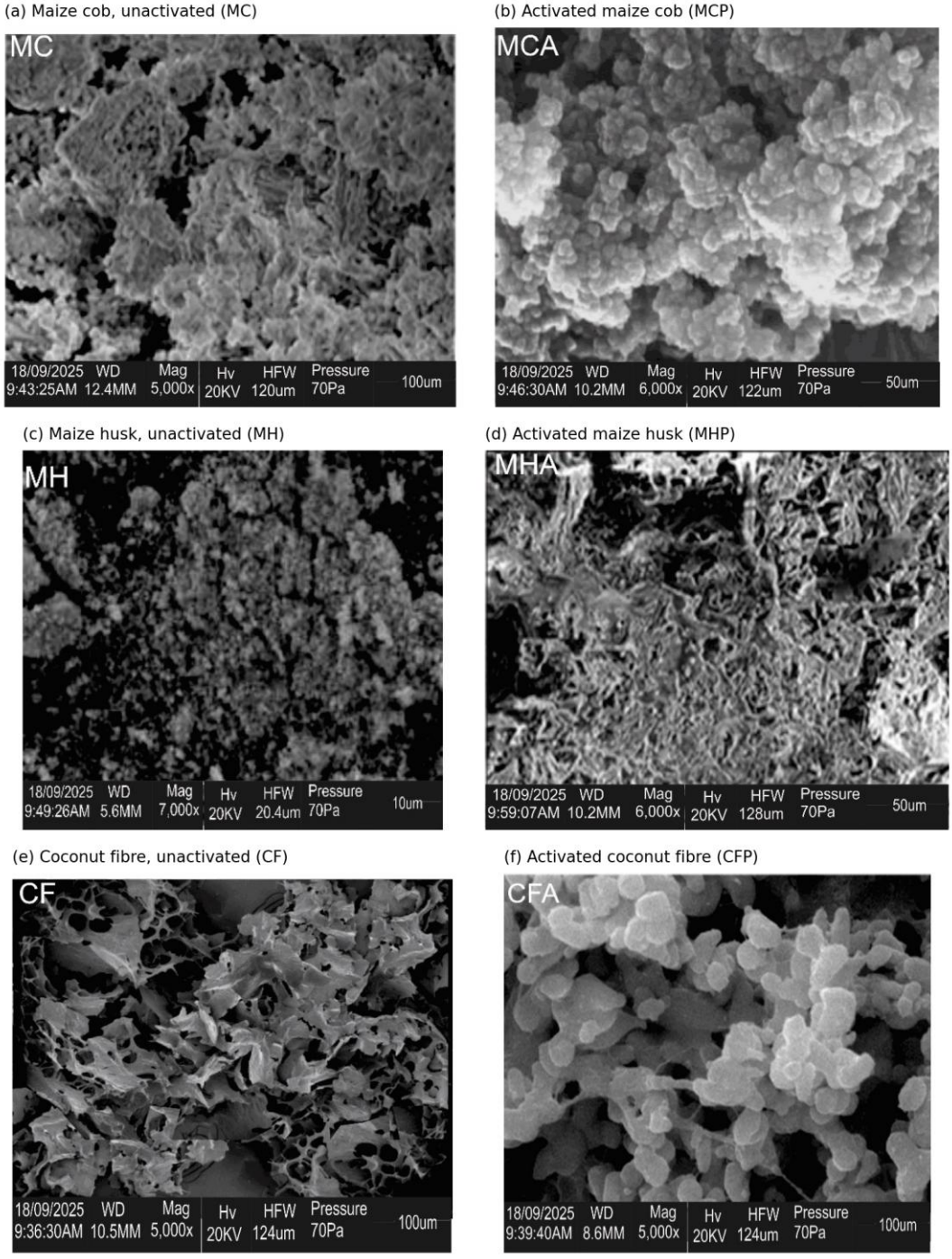


Figure 5. SEM micrographs of the unactivated chars (left) and the H_3PO_4-activated biochars (right): (a) maize cob (MC), (b) activated maize cob (MCP; laboratory ID MCA), (c) maize husk (MH), (d) activated maize husk (MHP; MHA), (e) coconut fiber (CF) and (f) activated coconut fiber (CFP; CFA). Magnification, field width, and scale bar are given on each micrograph (20 kV, low-vacuum mode, 70 Pa).

3.2 Effect of contact time and adsorption kinetics

Uptake of glyphosate (C_0 = 10 mg L^{-1}) rose quickly during the first 30 min and then changed little (Figure 6). After 120 min, the activated biochars removed 78.0% (MHA), 82.3% (MCA) and 87.7%

(CFA) of the glyphosate, giving q_e of 3.90, 4.12 and 4.39 mg g^{-1}, whereas the unactivated chars removed 35.0% (MH), 45.9% (MC) and 51.6% (CF), with q_e of 1.75, 2.30 and 2.58 mg g^{-1}. Activation therefore increased removal by about 2.2-fold for maize husk, 1.8-fold for maize cob, and 1.7-fold for coconut fiber, consistent with the larger surface area and pore volume of the activated biochars (Table 5). The unactivated MH plateaued after 50 min, whereas MC rose gently over the first 50 min. The unactivated CF showed almost constant uptake from the first reading (q_t about 2.3 mg g^{-1}), with a rise at 120 min, so the sampling times used did not resolve its kinetics; earlier sampling times would be needed.

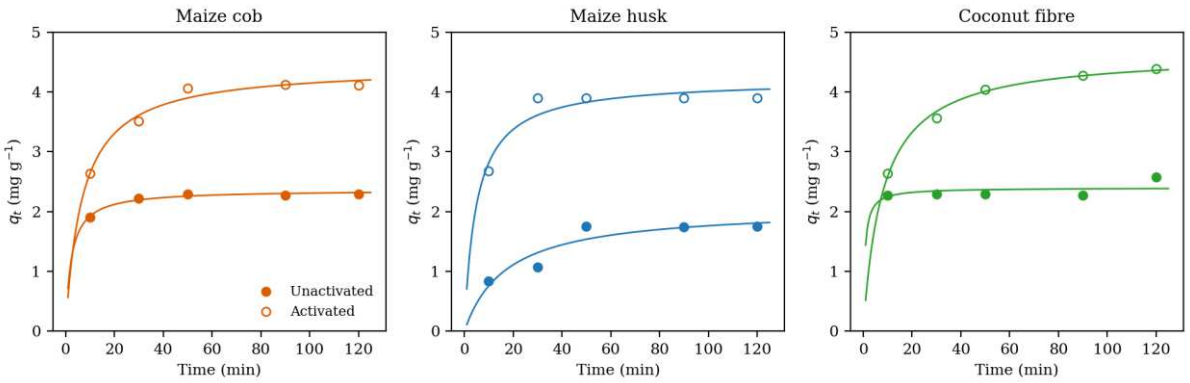


Figure 6. Effect of contact time on glyphosate uptake (C_0 = 10 mg L^{-1}, 2.0 g L^{-1}, natural pH (4.67); mean absorbance of three readings). Lines are pseudo-second-order fits.

Kinetic parameters from non-linear fits (Tables 6 and 7) rest on only five time points, and no single model described all six adsorbents. The pseudo-second-order model gave adjusted R^2 of 0.949 (MCA) and 0.983 (CFA), and the pseudo-first-order model gave the best fit for MHA (0.983); MC was described equally by both (0.938 and 0.939). MH was fitted poorly by all models (adj-R^2 up to 0.705), and none described the nearly flat uptake of CF (adj-R^2 below zero). Elovich and intraparticle-diffusion fits were generally weaker, and the Elovich α for MC and CF is not physically meaningful. Because several adsorbents reach their plateau within 30–50 min, there are too few points on the rising part of the curves to discriminate between models, and the rate constants are indicative only. The pseudo-second-order fit does not by itself show chemisorption (Tran et al., 2017).

For comparison, an H_3PO_4-oxidised corn cob biochar removed 44% of a commercial glyphosate formulation within 5 min (Marcelino et al., 2022), and a Mn/Fe-loaded activated carbon needed up to 24 h to reach equilibrium (Yamaguchi et al., 2019). The plateaus within 30–50 min found here are therefore at the fast end of the published range.

Table 6. Pseudo-first-order (PFO) and pseudo-second-order (PSO) parameters from non-linear fits (C_0 = 10 mg L^{-1}, five time points; $q_{e,exp}$ is the 120 min value).

Biochar	$q_{e,exp}$ (mg g^{-1})	PFO $q_{e,cal}$	PFO k_1 (min^{-1})	PFO adj-R^2	PSO $q_{e,cal}$	PSO k_2 (g mg^{-1} min^{-1})	PSO adj-R^2	PSO RMSE
MC	2.30	2.27	0.182	0.938	2.36	0.185	0.939	0.033

Biochar	$q_{e,exp}$ (mg g^{-1})	PFO $q_{e,cal}$	PFO k_1 (min^{-1})	PFO adj-R^2	PSO $q_{e,cal}$	PSO k_2 (g mg^{-1} min^{-1})	PSO adj-R^2	PSO RMSE
MCA	4.12	4.04	0.097	0.846	4.43	0.033	0.949	0.119
MH	1.75	1.78	0.046	0.680	2.07	0.028	0.705	0.197
MHA	3.90	3.93	0.116	0.983	4.21	0.048	0.779	0.210
CF	2.58	2.36	0.330	-0.825	2.40	0.628	-0.642	0.137
CFA	4.39	4.19	0.088	0.804	4.65	0.027	0.983	0.075

Table 7. Elovich and intraparticle diffusion (IPD) parameters from non-linear fits. n.m. = not meaningful (adj-R^2 below zero).

Biochar	Elovich α (mg g^{-1} min^{-1})	Elovich β (g mg^{-1})	Elovich adj-R^2	IPD k_{id} (mg g^{-1} $min^{-0.5}$)	IPD C (mg g^{-1})	IPD adj-R^2
MC	6.57e+03	6.57	0.633	0.043	1.89	0.322
MCA	5.27	1.60	0.822	0.184	2.36	0.585
MH	0.25	2.29	0.681	0.127	0.52	0.573
MHA	26.4	2.14	0.415	0.129	2.72	0.078
CF	n.m.	n.m.	-0.326	0.028	2.14	-0.110
CFA	3.1	1.39	0.948	0.217	2.21	0.783

3.3 Effect of initial concentration

Uptake increased with the initial concentration for all adsorbents (Figure 7, Table 8), and the activated biochars removed far more glyphosate than the unactivated chars at every concentration. The 50–500 mg L^{-1} calibration does not reach below 50 mg $L^{-1,}$ so that equilibrium concentrations could be quantified for only 14 of the 30 measurements; for the other 16, the absorbance was below that of the lowest standard and only $C_e < 50$ mg L^{-1}, and hence $q_e > (C_0 - 50)/2$, can be stated. At 500 mg L^{-1}, q_e was 224.8 (CFA), 214.6 (MCA) and 212.3 mg g^{-1} (MHA) for the activated biochars, against 159.2 (CF), 137.6 (MC) and 127.6 mg g^{-1} (MH) for the unactivated chars. With a dose of 2.0 g L^{-1}, the maximum possible uptake at 500 mg L^{-1} is 250 mg g^{-1}, so the activated biochars removed about 85–90% of the glyphosate even at the highest concentration, and the plateau was not reached. For this reason, and because most activated biochar points fall below the calibrated range, isotherm models (Table 3) could not be fitted reliably, and no maximum capacity (qm) is reported. Reported capacities for glyphosate adsorbents are mostly between about 0.6 and 125 mg g^{-1}: 1.49 mg g^{-1} for H_3PO_4-oxidised corn cob biochar (Marcelino et al., 2022), 9.19 mg g^{-1} for a Mn/Fe-loaded activated carbon (Yamaguchi et al., 2019), 27.5 mg g^{-1} for a porous clay heterostructure (Besghaier et al., 2022), 44.00 and 123.03 mg g^{-1} for a wood-derived and a steam-activated rice husk biochar (Herath et al., 2016), and 66.76 mg g^{-1} for an H_3PO_4-modified eucalyptus bark char at 373 K (Sen et al., 2019), although initial

concentrations, doses and glyphosate sources differ. The apparent uptake of at least 212 mg g−1 at 500 mg L−1 is higher than these values and is therefore provisional; confirmation with an independent analytical method and standards below 50 mg L^{-1} is recommended. Repeating at a lower dose or higher concentrations, with standards below 50 mg L^{-1}, would allow isotherm models to be fitted.

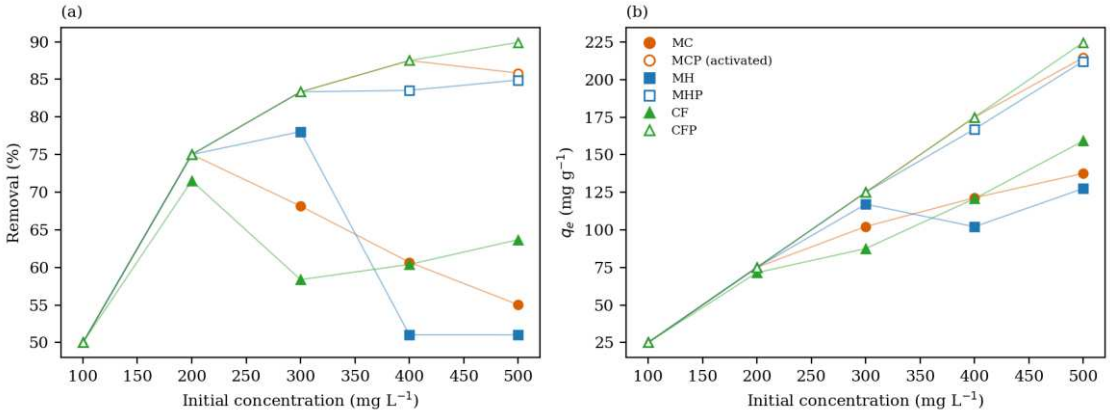


Figure 7. Effect of initial concentration at 120 min (2.0 g L^{-1}, natural pH (4.67)): (a) removal and (b) uptake. Triangles are lower bounds for samples below the calibrated range.

Table 8. Equilibrium concentration C_e (mg L^{-1}) / uptake q_e (mg g^{-1}) as a function of the initial concentration C_0 (mg L^{-1}). Entries of the form < 50 / > x are limits for samples below the calibrated range.

Biochar	**C_0 = 100**	**C_0 = 200**	**C_0 = 300**	**C_0 = 400**	**C_0 = 500**
MC	< 50 / > 25	< 50 / > 75	95.6 / 102.2	157.3 / 121.3	224.8 / 137.6
MCA	< 50 / > 25	< 50 / > 75	< 50 / > 125	< 50 / > 175	70.9 / 214.6
MH	< 50 / > 25	< 50 / > 75	65.8 / 117.1	195.9 / 102.1	244.9 / 127.6
MHA	< 50 / > 25	< 50 / > 75	< 50 / > 125	65.8 / 167.1	75.5 / 212.3
CF	< 50 / > 25	57.0 / 71.5	124.9 / 87.6	158.5 / 120.8	181.6 / 159.2
CFA	< 50 / > 25	< 50 / > 75	< 50 / > 125	< 50 / > 175	50.4 / 224.8

3.4 Effect of temperature and adsorption thermodynamics

For the activated biochars, removal of 10 mg L^{-1} glyphosate increased with temperature (Figure 8a): from 37.0 to 69.8% for MHA, from 22.0 to 64.3% for MCA and from 29.4 to 78.1% for CFA between 15 and 45 °C. The van't Hoff plots (Figure 8b) were linear over the three temperatures ($R^2 \geq 0.998$; Table 9). ΔG° was negative at all temperatures and became more negative with increasing temperature (from -7.6 to -15.1 kJ mol^{-1} across the three biochars), showing that adsorption is spontaneous and more favorable at higher temperatures. ΔH° was positive (34.8, 47.1 and 54.5 kJ mol^{-1} for MHA, MCA and CFA), indicating endothermic adsorption, and ΔS° was positive (153, 190 and 219 J mol^{-1} K^{-1}), which may reflect the release of water molecules from the surface and from solvated glyphosate on adsorption, increasing disorder at the solid–liquid interface. The ΔH° values are of the magnitude often attributed

to physisorption with a contribution from weaker chemical interactions. However, they are derived from one initial concentration and only three temperatures, so their standard errors (Table 9) understate the uncertainty.

Published thermodynamic results for glyphosate are mostly endothermic. A porous clay heterostructure took up more glyphosate between 25 and 50 °C, with positive ΔH° and negative ΔG° (Besghaier et al., 2022); an H_3PO_4-oxidised corn cob biochar was endothermic and endergonic with a commercial formulation (Marcelino et al., 2022); a Mn/Fe-loaded activated carbon gave ΔH° = +20.9 kJ mol^{-1} and ΔS° = −73.3 J mol^{-1} K^{-1} (Yamaguchi et al., 2019); and an H_3PO_4-modified eucalyptus bark char took up more glyphosate at higher temperature (Sen et al., 2019). The positive ΔH° (+35 to +55 kJ mol^{-1}) and negative ΔG° found here for the activated biochars agree in sign with these reports, whereas the positive ΔS° (+153 to +219 J mol^{-1} K^{-1}) is of opposite sign to, and larger than, the value reported by Yamaguchi et al. (2019). ΔH° values of this size are often read as a combination of physical and chemical interactions. However, Kc comes from a single initial concentration and three temperatures, so this reading is tentative.

For the unactivated chars, the absorbance at 15–45 °C (0.915–1.031) was at or above that of the 10 mg L^{-1} standard (0.926), so net removal could not be quantified in this series, and thermodynamic parameters are reported only for the activated biochars. Absorbance from compounds leached by the unactivated chars is a possible contribution at 210 nm. The temperature and time series were run as separate experiments, and removal at 30 °C in the temperature series (41–56% for the activated biochars) was lower than the 120 min removal in the room-temperature time series (78–88%); trends are therefore interpreted within each series.

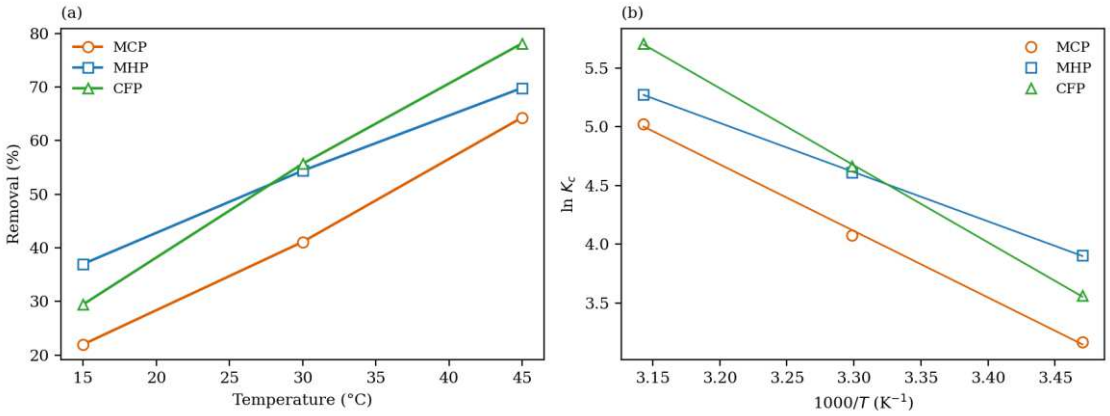


Figure 8. Effect of temperature for the activated biochars (C_0 = 10 mg L^{-1}, 2.0 g L^{-1}): (a) removal and (b) van't Hoff plots.

Table 9. Removal and thermodynamic parameters of the activated biochars (ΔG° in kJ mol^{-1}; ± are standard errors of the regression).

Biochar	Removal 15 °C (%)	Removal 30 °C (%)	Removal 45 °C (%)	ΔH° (kJ mol^{-1})	ΔS° (J mol^{-1} K^{-1})	ΔG° 288.15 K	ΔG° 303.15 K	ΔG° 318.15 K	R^2
MCA	22.0	41.1	64.3	47.1 ± 2.0	190 ± 6	-7.6	-10.3	-13.3	0.998
MHA	37.0	54.4	69.8	34.8 ± 0.3	153 ± 1	-9.4	-11.6	-14.0	1.000
CFA	29.4	55.7	78.1	54.5 ± 0.7	219 ± 2	-8.5	-11.8	-15.1	1.000

3.5 Surface evidence for the interaction

The FTIR spectra of the glyphosate-loaded biochars (Figure 4) show hydroxyl/amine, carbonyl, aromatic/carboxylate, and P–O-type bands on all six adsorbents, indicating these groups can interact with glyphosate. Without pre-adsorption spectra, it cannot be shown whether they participate in binding, and glyphosate itself contributes carboxylate and phosphonate bands in the same regions.

3.6 DFT analysis

3.6.1 Reactivity and geometry of glyphosate

The optimized glyphosate structure (B3LYP/6-31G, gas phase) is the neutral, non-zwitterionic form with all acidic hydrogens present (Figure 9, Table 10). The HOMO energy was -6.11 eV, and the LUMO energy was -0.41 eV, giving an energy gap of 5.70 eV. The chemical potential (-3.26 eV) and hardness (2.85 eV) describe a relatively hard, stable molecule, and the electrophilicity index of 1.86 eV indicates a moderate tendency to accept electrons. The computed dipole moment is 3.45 D. Mulliken charges identify the oxygen atoms as the most negative sites (−0.71 and −0.69 on the two P–OH oxygens, −0.64 on P=O, −0.54 on the carboxyl OH and −0.50 on C=O), with −0.61 on nitrogen and +1.49 on phosphorus, and the hydroxyl hydrogens (+0.38 to +0.40) and the N–H hydrogen (+0.30) as the most positive. These oxygen atoms are likely hydrogen-bond acceptor sites, and the O–H and N–H hydrogens are donor sites, which agrees with the red region on the electrostatic potential map (Figure 9c). Gas-phase calculations do not define a pH, so the neutral form is the reference species. In water at the natural pH of 4.67 of the solutions, glyphosate is mainly the monoanion, with a carboxylate, an ammonium, and one deprotonated phosphonate group (Figure 2), so these descriptors describe the isolated neutral molecule and do not capture pH-dependent speciation; calculations on the anionic and zwitterionic forms with an implicit solvent model are a natural extension. Selected calculated bond lengths and angles are given in Table 11.

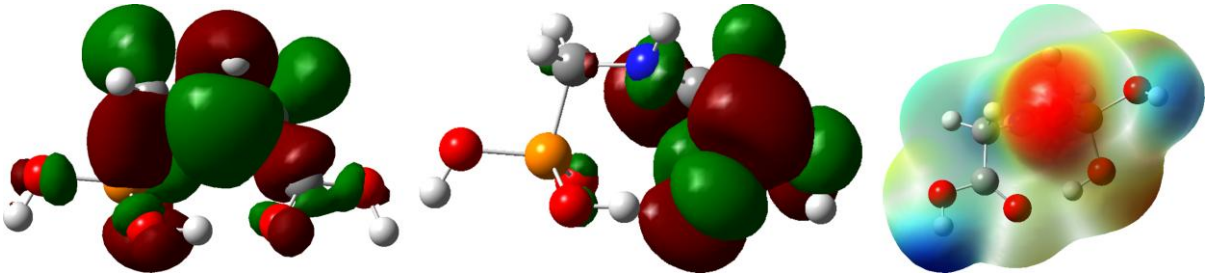


Figure 9. Optimized neutral glyphosate (B3LYP/6-31G, gas phase): (a) HOMO, (b) LUMO, and (c) molecular electrostatic potential map.

Table 10. Global reactivity descriptors of glyphosate from the optimized structure (B3LYP/6-31G). μ, η, ω, and σ are calculated here from the HOMO and LUMO energies.

Species	**E_{HOMO} (eV)**	**E_{LUMO} (eV)**	**ΔE (eV)**	**μ (eV)**	**η (eV)**	**ω (eV)**	**σ (eV^{-1})**	**Dipole moment (D)**
Neutral glyphosate	-6.11	-0.41	5.70	-3.26	2.85	1.86	0.35	3.45

Table 11. Selected bond lengths and angles of the optimized glyphosate (B3LYP/6-31G, gas phase), calculated from the optimized coordinates.

Parameter	**Value**	**Atoms**
P=O (Å)	1.567	P1=O6
P–OH (Å)	1.673, 1.661	P1–O2, P1–O4
P–C (Å)	1.852	P1–C7
C–N (Å)	1.461, 1.457	C7–N10, N10–C12
C–C (Å)	1.524	C12–C15
C=O (Å)	1.235	C15=O16
C–OH (Å)	1.365	C15–O17
O–H (Å)	0.994–1.020	O2–H3, O4–H5, O17–H18
N–H (Å)	1.013	N10–H11
C–H (Å)	1.092–1.101	C7–H, C12–H
O=P–OH (°)	116.3, 116.0	O6=P1–O2, O6=P1–O4
HO–P–OH (°)	103.6	O2–P1–O4
O=P–C (°)	114.4	O6=P1–C7
P–C–N (°)	107.1	P1–C7–N10
C–N–C (°)	119.9	C7–N10–C12
N–C–C (°)	110.1	N10–C12–C15
C–C=O (°)	126.9	C12–C15=O16

Parameter	Value	Atoms
O=C–OH (°)	121.9	O16=C15–O17

3.6.2 Adsorption energies on functional-group models (GFN2-xTB screening)

Adsorption energies of glyphosate on four functional-group models of the activated surface were screened with GFN2-xTB (Section 2.8.2; Table 12, Figure 10). For the glyphosate monoanion expected at the natural pH of 4.67, calculated in implicit water, E_{ads} was −19 kJ mol^{-1} on pristine coronene, −26 kJ mol^{-1} on the oxygenated model, −22 kJ mol^{-1} on the phosphorylated model, and −52 kJ mol^{-1} on the mixed model, with shortest heavy-atom contacts of 2.6–3.2 Å. These values are in the physisorption range, and only the mixed model, which carries both carboxyl and phosphate groups, gave a clearly stronger interaction. For neutral glyphosate in vacuum (the gas-phase calculation in Section 3.6.1), Eads was −37, −38, −53, and −108 kJ mol−1 for the four models, and implicit water weakened the interaction in the mixed model to −37 kJ mol−1 because the solvent competes for hydrogen bonds. The −37 kJ mol^{-1} (-0.38 eV) for pristine coronene lies within the −0.31 to −0.46 eV published for pristine and N-doped graphene (Table 13). The five starting orientations of each case differed by 9–91 kJ mol^{-1}, so the values are the best of a small sample and not converged global minima, and they are semi-empirical electronic energies without counterpoise or thermal corrections. B3LYP-D3 refinement of these geometries is planned.

Table 12. GFN2-xTB adsorption energies of glyphosate on functional-group models (kJ mol^{-1}; lowest of five optimizations). H-bonds and contacts are for the monoanion in water.

Model	Neutral, vacuum	Neutral, water	Monoanion (pH 4.67), water	Shortest heavy-atom contact (Å)	H-bonds
S0 pristine coronene	−37	−15	−19	3.03	0
S1: two OH, one COOH	−38	−32	−26	2.78	1
S2: two aryl phosphates	−53	−55	−22	3.19	1
S3 OH, COOH, aryl phosphate	−108	−37	−52	2.58	1

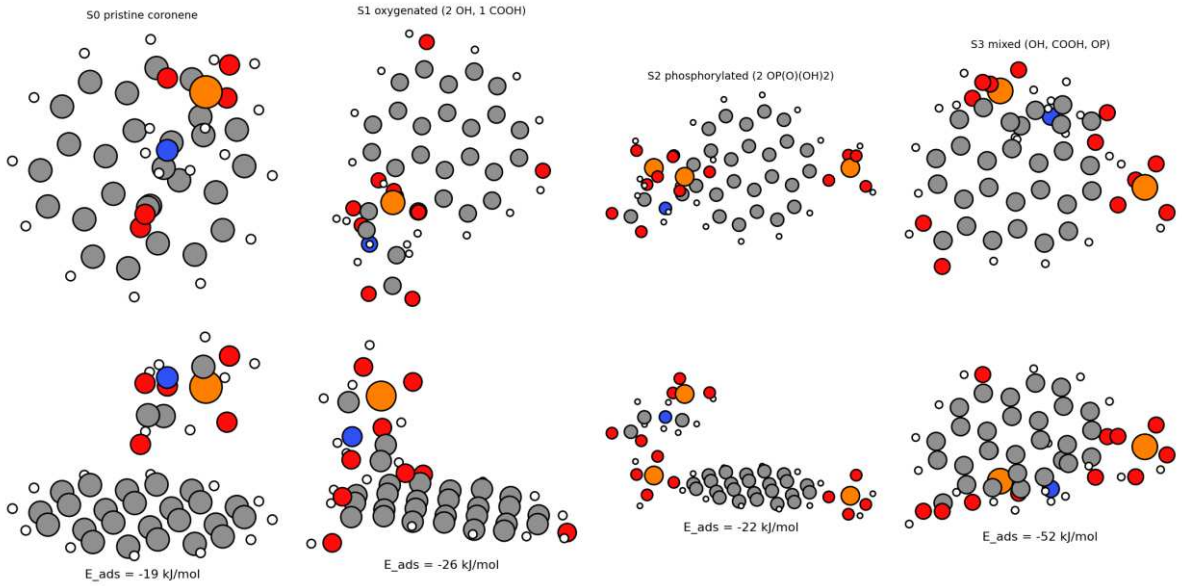


Figure 10. Lowest-energy complexes of the glyphosate monoanion with the four models in implicit water (GFN2-xTB; top and side views; grey C, white H, red O, blue N, orange P).

3.6.3 Published DFT adsorption energies of glyphosate (for comparison)

Published DFT studies on carbon-based surfaces give the following adsorption energies for comparison (Table 13). On pyridine-like nitrogen-doped graphene and on pristine graphene, glyphosate adsorbs weakly, with energies of about −0.31 eV (−30 kJ mol^{-1}) and −0.46 eV (−44 kJ mol^{-1}), which is physisorption, and decoration with Pt–Cu clusters strengthens this to −0.71 to −1.58 eV (−69 to −152 kJ mol^{-1}), the upper end being chemisorption (summarized by Hernández-Barreto et al., 2022). Doping graphene with Fe^{3+} or Al^{3+} enhances glyphosate binding through cooperative non-covalent and coordinative interactions (Mojica-Sánchez et al., 2026), and graphene-based materials with FTIR and Raman evidence show physisorption on pristine regions and chemisorption at vacancies (Araújo et al., 2024). The screening values found here, −19 to −52 kJ mol^{-1} for the monoanion in water and −37 to −108 kJ mol^{-1} for the neutral molecule in vacuum, fall in the lower part of this range, apart from the vacuum value for the mixed model. These are electronic energies at 0 K. The endothermic ΔH° found experimentally (+35 to +55 kJ mol^{-1}) is not in conflict with them, because adsorption from water also requires desolvation of glyphosate and of the surface, which gas-phase calculations omit.

Table 13. Published DFT adsorption energies of glyphosate on carbon-based surfaces (1 eV = 96.485 kJ mol^{-1}).

Surface	**E_{ads} (eV)**	**E_{ads} (kJ mol^{-1})**	**Interaction**	**Source**
Pyridine-like N-doped graphene	−0.31	−30	Physisorption	Hernández-Barreto et al., 2022
Pristine graphene (via the –NH group)	−0.46	−44	Very weak	Hernández-Barreto et al., 2022

Surface	E_{ads} (eV)	E_{ads} (kJ mol^{-1})	Interaction	Source
Pt–Cu clusters on N-doped graphene	−0.71 to −1.58	−69 to −152	Up to chemisorption	Hernández-Barreto et al., 2022
Fe^{3+}- and Al^{3+}-doped graphene	—	—	Enhanced; non-covalent and coordinative	Mojica-Sánchez et al., 2026
Graphene-based materials (pristine, doped, vacancies)	—	—	Physisorption; chemisorption at vacancies	Araújo et al., 2024

3.7 Proposed adsorption mechanism, comparison with published work and limitations

The measurements point to a surface-controlled, endothermic and entropy-driven uptake whose extent follows the development of porosity and surface groups (Table 14). Activation increased the surface area 3.7- to 8.2-fold, the pore volume 13- to 23-fold and the cation exchange capacity about 2-fold, and raised removal at 10 mg L^{-1} by a factor of 1.7–2.2. Gas-phase DFT identifies the oxygen atoms of glyphosate as the most negative sites, and its O–H and N–H hydrogens as donors, so hydrogen bonding and electrostatic interactions with surface hydroxyl, carboxyl, and phosphorus–oxygen groups, together with pore filling, are the most plausible interactions. The screening calculations support this: the glyphosate monoanion binds to the functional-group models with energies of −19 to −52 kJ mol^{-1}, strongest where carboxyl and phosphate groups are both present. These are the interaction types proposed for other glyphosate biochars (Herath et al., 2016), but here they are inferred from small model flakes with limited sampling, and the FTIR evidence cannot show which groups bind glyphosate.

Table 14. Evidence for the proposed adsorption mechanism.

Observation	Evidence	Interpretation
Uptake order CFA > MCA > MHA	q_e at 120 min (Section 3.2) and at 500 mg L^{-1} (Section 3.3); surface area and pore volume (Table 5)	Consistent with textural development; not separable from surface chemistry
Activation raises removal 1.7–2.2 times.	Section 3.2; Table 5 (area ×3.7–8.2, pore volume ×13–23, CEC ×2)	Activation creates more accessible sites
Plateau within 30–50 min	Section 3.2	Fast, surface-site-limited uptake; diffusion contribution undetermined
Endothermic, entropy-driven uptake	$\Delta H°$ +34.8 to +54.5 kJ mol^{-1}; $\Delta S°$ +153 to +219 J mol^{-1} K^{-1} (Table 9)	Consistent with desolvation and weak-to-moderate interactions; within the published range
Interaction sites of glyphosate	Gas-phase DFT: O atoms negative (−0.50 to −0.71), O–H and N–H hydrogens positive (+0.30 to +0.40); MEP (Table 10, Figure 9); GFN2-xTB E_{ads} −19 to −52 kJ mol^{-1} for the monoanion (Table 12)	Hydrogen bonding and electrostatic interaction with surface –OH, –COOH and P–O groups (hypothesis)

Observation	Evidence	Interpretation
Surface functional groups	FTIR bands of hydroxyl, carbonyl, carboxylate and P–O type groups (Figure 4)	Groups available for hydrogen bonding; their participation is not demonstrated

Limitations. The pH was not varied, so pH-dependent speciation and surface charge were not examined. Glyphosate-only and adsorbent-only controls were not included, and quantification relied on direct UV absorbance at 210 nm, which is not specific for glyphosate; contributions from other absorbing species cannot be excluded, and confirmation by an independent method (for example, derivatization or HPLC) would strengthen the quantitative results. We used two calibration curves with different slopes; the 50–500 mg L−1 curve does not extend below 50 mg L−1, and the absorbance values are means of three readings without reported standard deviations; therefore, we did not derive isotherm parameters, and the uptakes at 100–500 mg L^{-1} are provisional. The temperature series (120 min) gave lower removal at 30 °C than the room-temperature time series and no net removal for the unactivated chars, so the thermodynamic parameters apply to the activated biochars within that series and rest on one initial concentration and three temperatures. FTIR spectra before adsorption were not available. The DFT work consists of gas-phase B3LYP/6-31G calculations on neutral glyphosate, without a frequency calculation, and GFN2-xTB screening on small model flakes with five starting orientations per case, without counterpoise or thermal corrections; the proposed mechanism is therefore a hypothesis.

4. Conclusions

We prepared and tested H3PO4-activated biochars from maize cob, maize husk, and coconut fiber for glyphosate adsorption. Within the limitations described in Section 3.7, the main findings are:

- Activation raised the surface area (Sears titration) from 12.5–25.8 to 75.4–102.7 $m^2\ g^{-1}$ and the pore volume from 0.028–0.085 to 0.635–1.125 $cm^3\ g^{-1}$.
- At 10 mg L^{-1} and 2.0 g L^{-1}, the activated biochars removed 78.0–87.7% of the glyphosate in 120 min, compared with 35.0–51.6% for the unactivated chars; the uptake order was CFA > MCA > MHA, and the plateau was reached within 30–50 min.
- At 100–500 mg $L^{-1,}$ the apparent uptake of the activated biochars reached at least 212 mg g^{-1} at 500 mg L^{-1} without a plateau; this exceeds published capacities and is regarded as provisional, and isotherm parameters were not derived.
- For the activated biochars, uptake was spontaneous and endothermic (ΔG° −7.6 to −15.1 kJ mol^{-1}; ΔH° +34.8 to +54.5 kJ mol^{-1}), in the same direction as most published glyphosate studies.
- Gas-phase DFT of neutral glyphosate (B3LYP/6-31G) identified the oxygen atoms as the most negative sites, and GFN2-xTB screening on functional-group models gave adsorption energies of −19 to −52 kJ mol^{-1} for the monoanion at pH 4.67, in the physisorption range and within published values

for glyphosate on carbon-based surfaces, with the strongest binding where carboxyl and phosphate groups are both present.

- These results indicate that H_3PO_4-activated agricultural-residue biochars are of interest for glyphosate removal; confirmation with controls, pH measurements, an independent analytical method, calibration standards below 50 mg L^{-1}, spectra before adsorption, and DFT refinement of the adsorption energies are the next steps.

Declarations

Author contributions (CRediT)

Author	CRediT roles	Contribution to this work
Author 1 (first and corresponding author)	Conceptualization; Methodology; Investigation; Formal analysis; Software; Visualization; Writing – original draft	Designed the study; carried out and analyzed the batch adsorption experiments; performed kinetic and thermodynamic modeling; conducted gas-phase DFT and adsorption-screening calculations; prepared figures and tables; wrote the original draft.
Author 2 (senior and corresponding author)	Conceptualization; Supervision; Project administration; Resources; Funding acquisition; Writing – review and editing	Conceived the project, supervised the study, administered the project and resources, and critically revised the manuscript.
Author 3	Investigation; Validation; Data curation	Carried out the batch experiments and UV measurements; prepared the standards and calibration curves; verified the raw data.
Author 4	Software; Formal analysis; Validation; Writing – review and editing	Advised on and checked the computational chemistry (DFT and semi-empirical models) and reviewed the interpretation of the computed results.
Author 5	Methodology; Validation; Supervision; Writing – review and editing	Supervised the experimental work and the analytical methodology; reviewed the data analysis and its interpretation.
Author 6	Investigation; Resources; Data curation; Writing – review and editing	Prepared the H_3PO_4-activated and unactivated chars; coordinated the physical and FTIR characterization; curated the laboratory data.

All authors read and approved the final manuscript and agree to be accountable for all aspects of the work.

Funding

This research received no specific grant from any funding agency in the public, commercial or not-for-profit sectors.

Competing interests

The authors declare that they have no known competing financial interests or personal relationships that could have influenced the work reported in this paper.

Declaration of limitations

The authors declare the following limitations of this study. (1) The experiments were run at the natural solution pH (4.67) only, and no glyphosate-only or adsorbent-only controls were included. (2) Glyphosate was quantified by direct UV absorbance at 210 nm, which is not specific for glyphosate, and the 50–500 mg L^{-1} calibration does not extend below 50 mg L^{-1}. The uptake at 100–500 mg L^{-1} is therefore provisional and no isotherm parameters were derived. (3) The thermodynamic parameters were obtained from one initial concentration at three temperatures and apply to the activated biochars only. (4) The DFT and GFN2-xTB calculations were gas-phase or implicit-solvent screenings on model surfaces, so the proposed adsorption mechanism is a hypothesis. The authors plan to address these points in follow-up work with controls, a wider pH range, an independent analytical method and DFT refinement.

Data availability

The raw absorbance readings, calibration standards, FTIR spectra, the Gaussian output for glyphosate and the GFN2-xTB structures, scripts and Gaussian input files are available as Supplementary Information.

Use of generative AI

During the preparation of this manuscript, the authors used Claude (Anthropic) and Grammarly to assist with language editing, compilation, preparation of figures and tables, and the GFN2-xTB screening calculations, whose structures, scripts, and outputs are provided. The authors reviewed and verified all content and take full responsibility for it. No AI tool is listed as an author.

Ethics, Consent to Participate, and Consent to Publish

Not applicable

Acknowledgements

The Authors acknowledge the Springboard Analytical Laboratory, Awka, Nigeria, which performed the surface-property and UV measurements for this work.

References

Agency for Toxic Substances and Disease Registry (ATSDR). (2021). Chemical and physical information. In Toxicological profile for glyphosate (Chapter 4). U.S. Department of Health and Human Services. https://www.atsdr.cdc.gov/toxprofiles/tp214-c4.pdf

Akama, S., Yamamura, M., & Kigawa, T. (2012). A Multiphysics Model of In Vitro Transcription Coupling Enzymatic Reaction and Precipitation Formation. https://doi.org/10.1016/j.bpj.2011.12.014

Alarape, S. A., Fagbohun, A. F., Ipadeola, O. A., Adeigbo, A. A., Adesola, R. O., & Adeyemo, O. K. (2023). Assessment of glyphosate and its metabolites' residue concentrations in cultured African catfish offered for sale in selected markets in Ibadan, Oyo State, Nigeria. Frontiers in Toxicology, 5, 1250137. https://doi.org/10.3389/ftox.2023.1250137

Araújo, W. S., Rêgo, C. R. C., Guedes-Sobrinho, D., Dias, A. C., do Couto, I. R., Bordin, J. R., de Matos, C. F., & Piotrowski, M. J. (2024). Quantum simulations and experimental insights into glyphosate adsorption using graphene-based nanomaterials. ACS Applied Materials & Interfaces, 16(24): 31500–31512. https://doi.org/10.1021/acsami.4c05733

Bai, S. H., & Ogbourne, S. M. (2016). Glyphosate: environmental contamination, toxicity and potential risks to human health via food contamination. Environmental Science and Pollution Research, 23(19), 18988–19001.

Battaglin, W. A., Meyer, M. T., Kuivila, K. M., & Dietze, J. E. (2014). Glyphosate and its degradation product AMPA occur frequently and widely in U.S. soils, surface water, groundwater, and

precipitation. Journal of the American Water Resources Association, 50, 275–290. https://doi.org/10.1111/jawr.12159

Becke, A. D. (1993). Density-functional thermochemistry. III. The role of exact exchange. Journal of Chemical Physics, 98, 5648–5652. https://doi.org/10.1063/1.464913

Besghaier, S., Cecilia, J. A., Chouikhi, N., Vilarrasa-García, E., Rodríguez-Castellón, E., Chlendi, M., & Bagane, M. (2022). Glyphosate adsorption onto porous clay heterostructure (PCH): kinetic and thermodynamic studies. Brazilian Journal of Chemical Engineering, 39(4), 903–917. https://doi.org/10.1007/s43153-021-00166-7

Bhaskara, B. L., & Nagaraja, P. (2006). Direct sensitive spectrophotometric determination of glyphosate by using ninhydrin as a chromogenic reagent in formulations and environmental water samples. Helvetica Chimica Acta, 89, 2686–2693.

Borggaard, O. K., & Gimsing, A. L. (2008). Fate of glyphosate in soil and the possibility of leaching to ground and surface waters: a review. Pest Management Science, 64(4), 441–456.

Cosgrove, S., Jefferson, B., & Jarvis, P. (2019). Pesticide removal from drinking water sources by adsorption: a review. Environmental Technology Reviews, 8(1), 1–24.

Frisch, M. J., Trucks, G. W., Schlegel, H. B., Scuseria, G. E., Robb, M. A., Cheeseman, J. R., Scalmani, G., Barone, V., Mennucci, B., Petersson, G. A., Nakatsuji, H., Caricato, M., Li, X., Hratchian, H. P., Izmaylov, A. F., Bloino, J., Zheng, G., Sonnenberg, J. L., Hada, M., . . . Fox, D. J. (2013). Gaussian 09 (Revision D.01) [Computer software]. Gaussian, Inc.

Guyton, K. Z., Loomis, D., Grosse, Y., et al. (2015). Carcinogenicity of tetrachlorvinphos, parathion, malathion, diazinon, and glyphosate. The Lancet Oncology, 16(5), 490–491. https://doi.org/10.1016/S1470-2045(15)70134-8

Herath, I., Kumarathilaka, P., Al-Wabel, M. I., Abduljabbar, A., Ahmad, M., Usman, A. R. A., & Vithanage, M. (2016). Mechanistic modeling of glyphosate interaction with rice husk derived engineered biochar. Microporous and Mesoporous Materials, 225, 280–288. https://doi.org/10.1016/j.micromeso.2016.01.017

Hernández-Barreto, D. F., Bernal, V., Giraldo, L., Moreno-Piraján, J. C., & Rodriguez-Estupiñán, P. (2022). Biomass valorization by thermal treatments: Graphene-based materials and their application on glyphosate adsorption. Frontiers in Sustainability, 3, 926438. https://doi.org/10.3389/frsus.2022.926438

Ho, Y. S., & McKay, G. (1999). Pseudo-second order model for sorption processes. Process Biochemistry, 34, 451–465.

Ighalo, J. O., Ajala, O. J., Adeniyi, A. G., Babatunde, E. O., & Ajala, M. A. (2021). Ecotoxicology of glyphosate and recent advances in its mitigation by adsorption. Environmental Science and Pollution Research, 28, 2655–2668.

Ioannidou, O., & Zabaniotou, A. (2007). Agricultural residues as precursors for activated carbon production — A review. Renewable and Sustainable Energy Reviews, 11(9), 1966–2005.

Jagtoyen, M., & Derbyshire, F. (1993). Activated carbons from yellow poplar and white oak by H_3PO_4 activation. Carbon, 31(7), 1185–1197.

Lagergren, S. (1898). About the theory of so-called adsorption of soluble substances. Kungliga Svenska Vetenskapsakademiens Handlingar, 24(4), 1–39.

Lee, C., Yang, W., & Parr, R. G. (1988). Development of the Colle-Salvetti correlation-energy formula into a functional of the electron density. Physical Review B, 37, 785–789.

Lima, E. C., Hosseini-Bandegharaei, A., Moreno-Piraján, J. C., & Anastopoulos, I. (2019). A critical review of the estimation of the thermodynamic parameters on adsorption equilibria. Wrong use of equilibrium constant in the Van't Hoof equation for calculation of thermodynamic parameters of adsorption. Journal of Molecular Liquids, 273, 425–434. https://doi.org/10.1016/j.molliq.2018.10.048

Lita, A. L., Hidayat, E., Mohamad Sarbani, N. M., Harada, H., Yonemura, S., Mitoma, Y., Herviyanti, & Gusmini. (2023). Glyphosate removal from water using biochar based coffee husk loaded Fe_3O_4. Water, 15(16), 2945. https://doi.org/10.3390/w15162945

Liu, B., Dong, L., Yu, Q., Li, X., Wu, F., Tan, Z., & Luo, S. (2016). Thermodynamic study on the protonation reactions of glyphosate in aqueous solution: potentiometry, calorimetry and NMR spectroscopy. Journal of Physical Chemistry B, 120(9), 2132–2137.

Marcelino, N. V. A., dos Santos, H. V. R., Cuba, R. M. F., & Cuba Teran, F. J. (2022). Effect of H3PO4 oxidation of corn cob biochar on the adsorption of a commercial glyphosate formulation. Desalination and Water Treatment, 274, 102–114. https://doi.org/10.5004/dwt.2022.28801

Mayakaduwa, S. S., Kumarathilaka, P., Herath, I., Ahmad, M., Al-Wabel, M., Ok, Y. S., Usman, A., Abduljabbar, A., & Vithanage, M. (2016). Equilibrium and kinetic mechanisms of woody biochar on aqueous glyphosate removal. Chemosphere, 144, 2516–2521.

Mojica-Sánchez, J. P., González-Ramírez, H. N., Nochebuena, J., Ruiz-Ibarra, G., & Medel-Juarez, V. M. (2026). Metal-doped graphene as adsorbents for glyphosate: a DFT and molecular dynamics approach. Australian Journal of Chemistry, 79, CH25136. https://doi.org/10.1071/CH25136

National Center for Biotechnology Information. (2026). PubChem compound summary for CID 3496, Glyphosate. https://pubchem.ncbi.nlm.nih.gov/compound/Glyphosate (retrieved October 9, 2026).

Oyetunji, G. O., Olagunju, E. A., Ajayi, O. O., & Adesina, G. O. (2024). Herbicide use in Nigeria: a review of its effects on human, animal, and environmental health. Journal of Applied Life Sciences and Environment, 57(4), 545–590. https://doi.org/10.46909/alse-574152

Parr, R. G., & Pearson, R. G. (1983). Absolute hardness: companion parameter to absolute electronegativity. Journal of the American Chemical Society, 105, 7512–7516.

Parr, R. G., von Szentpály, L., & Liu, S. (1999). Electrophilicity index. Journal of the American Chemical Society, 121, 1922–1924.

Sears, G. W. (1956). Determination of specific surface area of colloidal silica by titration with sodium hydroxide. Analytical Chemistry, 28(12), 1981–1983.

Sen, K., Datta, J. K., & Mondal, N. K. (2019). Glyphosate adsorption by Eucalyptus camaldulensis bark-mediated char and optimization through response surface modeling. Applied Water Science, 9, 162. https://doi.org/10.1007/s13201-019-1036-3

Tran, H. N., You, S.-J., Hosseini-Bandegharaei, A., & Chao, H.-P. (2017). Mistakes and inconsistencies regarding adsorption of contaminants from aqueous solutions: A critical review. Water Research, 120, 88–116.

Tzilivakis, J., Lewis, K. A., Green, A., & Warner, D. J. (2026). Glyphosate (Ref: MON 0573). Pesticide Properties DataBase. University of Hertfordshire. (retrieved October 9, 2026).

Yakout, S. M., & Sharaf El-Deen, G. (2016). Characterization of activated carbon prepared by phosphoric acid activation of olive stones. Arabian Journal of Chemistry, 9, S1155–S1162.

Yamaguchi, N. U., Rubio, A. J., & Bergamasco, R. (2019). Activated carbon loaded with manganese and iron for glyphosate adsorption: Kinetics, isotherms and thermodynamic studies. Revista Ambiente & Água, 14(6), e2414. https://doi.org/10.4136/ambi-agua.2414

Zaparoli, M., Igansi, A. V., da Silveira, J. T., de Morais, M. G., & Costa, J. A. V. (2023). Biochar as a sustainable alternative for the use of residues from the processing of açaí and the removal of glyphosate. Journal of Environmental Chemical Engineering, 11(6), 111162. https://doi.org/10.1016/j.jece.2023.111162